RSC Advances

This is an *Accepted Manuscript*, which has been through the Royal Society of Chemistry peer review process and has been accepted for publication.

Accepted Manuscripts are published online shortly after acceptance, before technical editing, formatting and proof reading. Using this free service, authors can make their results available to the community, in citable form, before we publish the edited article. This *Accepted Manuscript* will be replaced by the edited, formatted and paginated article as soon as this is available.

You can find more information about *Accepted Manuscripts* in the Information for Authors.

Please note that technical editing may introduce minor changes to the text and/or graphics, which may alter content. The journal's standard Terms & Conditions and the Ethical guidelines still apply. In no event shall the Royal Society of Chemistry be held responsible for any errors or omissions in this *Accepted Manuscript* or any consequences arising from the use of any information it contains.

ROYAL SOCIETY OF CHEMISTRY

www.rsc.org/advances

Please do not adjust margins

Journal Name

ARTICLE

Organic dyes for the sensitization of nanostructured ZnO photoanodes: effect of the anchoring functions

Received 00th January 20xx,
Accepted 00th January 20xx

DOI: 10.1039/x0xx00000x

www.rsc.org/

J. Idígoras,[a*] M. Godfroy,[b,c,d] D. Joly,[b,c,d] A. Todinova,[a] P. Maldivi,[e,f] G. Oskam,[g] R. Demadrille[b,c,d] and J. A. Anta[a]

Among all n-type metal oxide semiconductors that can be used in solar cells as photoanode, ZnO is one of the most appealing alternatives to the ubiquitous TiO_2. This material offers some potentially favourable characteristics with respe to TiO_2, such as higher electron mobility in the bulk and a rich variety of nanostructures. However, ZnO has certain drawbacks as photoanode material, for example, a poor chemical stability and a slower charge separation process at the ZnO interface that reduces the electron injection rate. Therefore, in the case of dye-sensitized solar cells, the search of new dyes with a higher light harvesting efficiency and specifically designed to bind to ZnO can be considered as a possible strategy to improve performance in systems characterized by a low electron injection rate. In this work the optical, electrochemical and photovoltaic properties of a family of purely organic sensitizers with various anchoring groups have been investigated and compared with the most commonly used ruthenium dye **N719**. In particular, we have shown that the structurally simple organic dye coded **RK1** is an excellent sensitizer for ZnO photoanodes. Thanks to this molecule, the energy conversion efficiency under standard conditions (1 sun AM 1.5 illumination) employing ZnO-based photoanodes reached 3.7%, which is more than two times higher than obtained with the **N719** dye studied under the same conditions.

Introduction

Among all components of a Dye-Sensitized Solar Cell (DSSC),[1,2] the function of light absorption and charge separation by means of electron injection in the semiconductor is carried out by the sensitizer dye molecules. However, not only the generation of an electric current depends on the properties of the dye, but also the electron recombination with the oxidized species present in the electrolyte, which determines the photovoltage of solar devices.[3] Therefore, bearing in mind the importance of dyes in the global performance of DSSC, the study and development of new sensitizers have received much interest. Among them one can cite the ruthenium-containing dyes such as polypyridyl complexes, the metallated porphyrins and the fully organic dyes. Recently, a clear breakthrough in the field has been the use of lead perovskites in solar cells.[4–6]

Since the origins of DSSCs, the most employed dyes are ones containing ruthenium complexes, which have demonstrated high efficiencies. These dye molecules are characterized by the occurrence of a Metal-to-Ligand Charge Transfer (MLCT) feature with a wide absorption spectrum and a moderate absorption coefficient.[7] The latter characteristic has negative influence on the performance of these dyes in solar cells with ionic liquids or solid hole conductors as electrolytes, where the mass transfer limitation and the rapid recombination requires very thin films as photoanodes. As an additional drawback, the dyes containing ruthenium, an exceedingly rare metal, are associated with high fabrication costs. Nevertheless, the ruthenium dyes show a long excited-state lifetime, a good electrochemical stability under illumination and appropriate energy levels (LUMO and HOMO) for an efficient electron injection and for rapid dye regeneration when TiO_2 nanostructures are used as photoanodes.

In the search and development of new sensitizers, fully organic dyes, which are characterized by a high absorption coefficient,[8] have extensively been studied. Up to date numerous papers demonstrate efficiencies of DSSCs comparable to the ones where ruthenium dyes are used. For instance, efficiencies of 10.1% (**C219**)[9] and 12.3% (co-sensitization by **YD2-o-C8** porphyrin dye and other organic **Y123** dye)[10] have been achieved under simulated 1 sun AM 1.5 global sunlight. The advantage of these dyes, among other properties, is not only their high absorption coefficients, but also the low production costs and the possibility to modify the routes of synthesis and to change the absorption spectrum by the incorporation of new groups.[11,12]

[a] Área de Química Física, Departamento de Sistemas Físicos, Químicos y Naturales, Universidad Pablo de Olavide, E-41013, Seville, Spain.
[b] Univ. Grenoble Alpes, INAC-SPRAM, F-38000 Grenoble, France.
[c] CNRS, Alpes, INAC-SPRAM, F-38000 Grenoble, France.
[d] CEA, INAC-SPRAM, F-38000 Grenoble, France.
[e] Univ. Grenoble Alpes, INAC-SCIB, F-38000 Grenoble, France.
[f] CEA, INAC-SCIB, F-38000 Grenoble, France.
[g] Departamento de Física Aplicada, CINVESTAV-IPN, 97310, Mérida, Yucatán, México.

† Footnotes relating to the title and/or authors should appear here.

Electronic Supplementary Information (ESI) available: Details of LUMO position for the dyes, the J-V curves for different conditions for ZnO-DSSCs, the J-V curves and data information as extracted from impedance spectroscopy for TiO_2-DSSCs, voltage decays and SEM imagen for ZnO films. See DOI: 10.1039/x0xx00000x

RSC Advances Accepted Manuscript

Please do not adjust margins

Among organic dyes, the family of *Donor-π-Acceptor* (*D-π-A*) dyes has received increased attention due to easier modification of the chemical structure.[9,13–16] These dyes result from the combination of two units linked covalently through a spacer (*π-bridge*). One of them is an *electron donor* group, whose aim is to increase light absorption and to facilitate regeneration of the dye, whereas the other unit is an *electron acceptor* group, which favours electron injection in the semiconductor after the intramolecular charge transfer from electron donor group. Thanks to this molecular design it is possible to create new dyes modifying the chemical structure of each unit.

In this work, we study the photovoltaic performances of nanostructured ZnO photoanodes sensitized with different organic D-π-A dyes that we compare to a reference compound i.e. the ruthenium complex coded **N719**. All the organic dyes employed in this study (**Figure 1**) are derived from the same π-conjugated system inspired by the dye (**RK1**), for which an efficiency of over 10% has been demonstrated on TiO_2.[17] Owing to the good performances of this dye, our objective in this work was to assess its potential with ZnO electrodes and to adapt its chemical structure in order to investigate the interfacial processes that govern the generation of current in this type of solar cells. Indeed despite of the fact that many organic dyes have been published in the recent years,[14–16] the literature dealing with the tuning of their chemical structure specifically for the sensitization of ZnO electrode is very scarce. In particular, the main differences between these organic dyes is related to the substitution of the triphenyl amine with alkoxy groups and/or the number and nature of the anchoring groups, standing out the **MG100** dye by the presence of a phosphoric acid group specifically adapted to bind to ZnO.

At this point it is important to mention the limitations of the application of ZnO electrodes as photoanodes in DSSC. In previous works it has been discussed that ZnO-based solar cells show worse performance with respect to TiO_2-based solar cells as a consequence of the lower electron injection rate, slower dye regeneration and/or the presence of an intermediate state of the dye with strong back recombination.[18,19] In addition, ZnO electrodes show a high instability in the presence of ruthenium dyes, such as N719 or other acidic dyes. A partial dissolution of the semiconductor and the formation of dye-ZnO aggregates have been evidenced after the immersion in acidic dye solution.[20–24] Nevertheless, the record efficiency for ZnO-based solar cells (7.5%) has been achieved using hierarchically assembled ZnO nanocrystallites deposited on a ZnO buffer layer and **N719** as the sensitizer.[25] However, efficiencies higher than 5% were achieved using ZnO nanowires sensitized by SK1 (D-π-A dye) in combination with cobalt complex as redox shuttle.[26] In this work, DSSCs were fabricated using ZnO nanoparticles as photoanodes sensitized with the different organic dyes. Among them the sensitizer coded **RK1** has shown the highest performances and a twice as high power conversion efficiency in comparison to the DSSCs containing ruthenium dye.

Results and discussion

Synthesis of the dyes.

In this work we have used as reference materials two dyes from the RK series that have demonstrated power conversion efficiencies of over 10% for mesoporous TiO_2 electrodes in DSSC configuration.[27] In addition, two new dyes were synthesized differing by the nature and the number of anchoring functions.

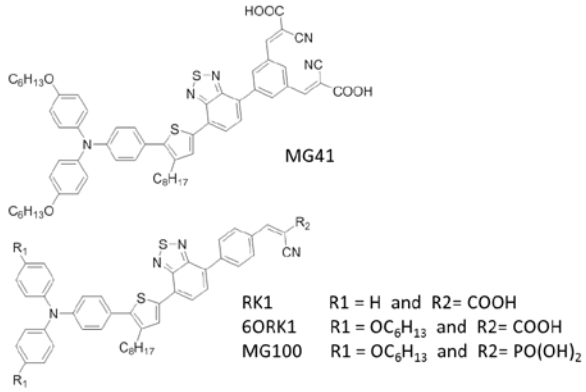

Fig. 1: Structure of the organic dyes employed in this work.

MG41 that contains a double anchoring cyanoacrylic acid group and **MG100**, with a cyanovinylphosphonic group (**Scheme 1**).The dyes were synthesized in three steps through classical cross-coupling reactions under Stille or Suzuki conditions. The introduction of the anchoring groups was performed using Knoevenagel condensations. For **MG100**, the cleavage of the phosphonate group was achieved using iodo-trimethylsilane following standard procedure.[28]

Optical and electrochemical characterisations.

The UV-Vis spectra of the solution of the organic dyes in dichloromethane are shown in **Figure 2A**. The spectra are characterised by the presence of two absorption bands. The most intensive band located in the UV region is associated with the high-energy π-π* orbital transition. On the other hand, the band located in the visible region is associated with the intramolecular charge transfer from the electron donor to the electron acceptor group. For **RK1**, **6ORK1**, **MG41** and **MG100** dyes, the latter absorption band exhibits absorption maxima at 481, 503, 492 and 492 nm, respectively, with a molar absorption coefficient of 29800, 20000, 11200 and 12300 $M^{-1}cm^{-1}$ (**Table 1**). As expected, the intensity and the position of the ICT bands are dependent on the modification of the chemical structure.[12] Indeed, the introduction of two electron-donating alkoxy-substituents on the TPA unit induces a bathochromic shift of the ICT band for all the dyes compared to **RK1**. Simultaneously, the molar extinction coefficients are decreased for these three dyes due to the additional alkyl chains that do not contribute to the absorption. In the case of **MG41** and **MG100**, the less effective conjugation of the anchoring functions with the rest of the π-conjugated system (also demonstrated by theoretical calculations) explains their much lower molar absorption coefficients.

RSC Advances Accepted Manuscript

 This journal is © The Royal Society of Chemistry 20xx

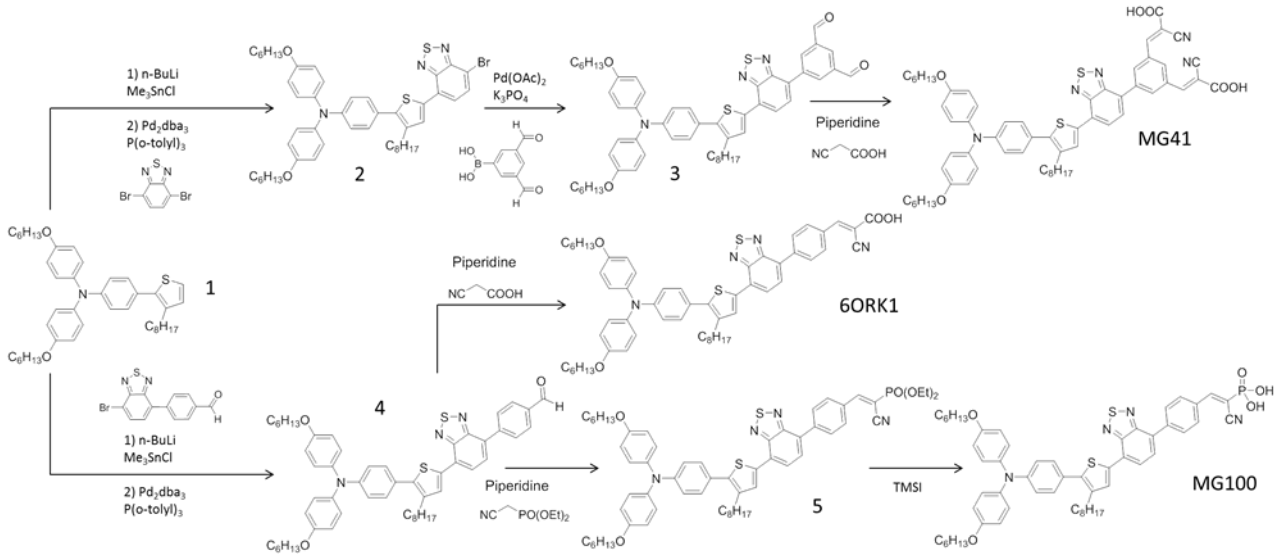

Scheme 1: Synthesis of the dyes studied in this work

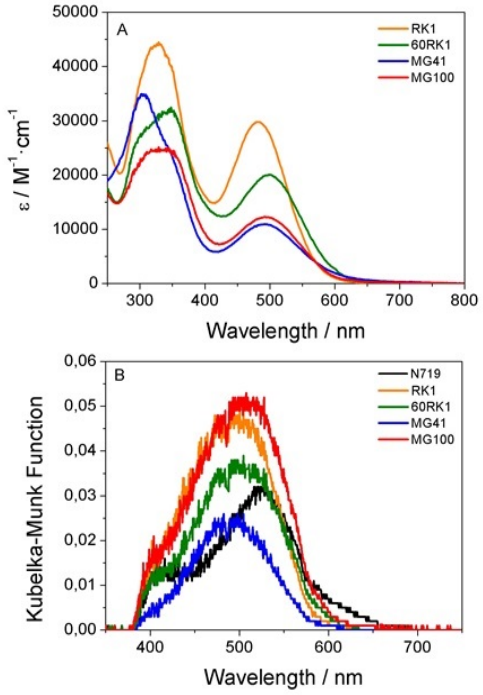

Fig. 2: (A) UV-Vis spectra of synthesized dyes studied in dichloromethane and (B)adsorbed onto the ZnO surface.

Assuming that all photoanodes have the same surface area, a higher molar absorption coefficient should be correlated with a higher absorption signal, as shown in **Figure 2B** for **RK1- 6ORK1** and **MG41-**ZnO photoanodes. Nevertheless, the **MG100-**ZnO photoanode shows an absorption maximum very similar to that for the **RK1-**ZnO photoanode (0.05 and 0.044, respectively), whereas the absorption coefficient for **MG100-**ZnO is almost three times smaller (**Figure 2A**). Therefore, a higher concentration of dye molecules on ZnO surface may be inferred from the results in the case of **MG100-**ZnO.

In order to determine the position of the LUMO and HOMO levels of the organic dyes an electrochemical study was performed by means of cyclic voltammetry (**Table 1**). Both energy levels were determined from the oxidation and reduction onset with respect to NHE. The band gap energy was determined by the energy difference between the levels. Although the HOMO-LUMO difference does not necessarily corresponds to the energy absorption onset, it is still a good approximation for the energy difference between ground and excited state. A value of the band gap of around 1.7-2.0 eV confirms that the organic dyes have a relatively strong absorption in the visible range of wavelengths.

To compare these experimental values and to gain insight into structural properties, the electron density distribution of the

Table 1: Photophysical data: (a) Measured in CH_2Cl_2, (b) determined from the onset of the first oxidation and reduction (c) calculated *Eg*= HOMO – LUMO. All potentials were obtained during cyclic voltammetric investigations in 0.2 M Bu_4NPF_6 in CH_2Cl_2. Potentials measured vs Fc^+/Fc were converted to NHE by addition of +0.69 V. Platinum electrode diameter was 1 mm, sweep rate: 200 mV s^{-1}. (d) Calculated at B3LYP level of theory.

Dye	λ_{abs} [(a)] (nm)	ε [(a)] ($M^{-1}cm^{-1}$)	HOMO[(b)] (V vs NHE)	LUMO[(b)] (V vs NHE)	*Eg*[(c)] (eV)	HOMO[(d)] (V vs NHE)	LUMO[(d)] (V vs NHE)	*Eg*[(d)] (eV)
RK1	481	29800	0.76	-1.22	1.98	0.73	-1.28	1.91
6ORK1	503	20000	0.53	-1.16	1.69	0.59	-1.23	1.82
MG41	492	11200	0.52	-1.22	1.74	0.54	-1.36	1.90
MG100	492	12300	0.48	-1.24	1.72	0.53	-1.35	1.88

RSC Advances Accepted Manuscript

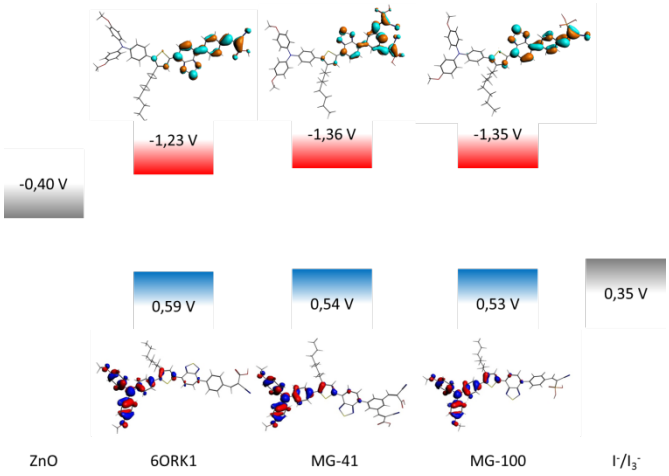

Fig. 3: Frontier molecular orbitals of the dyes calculated at B3LYP level of theory.

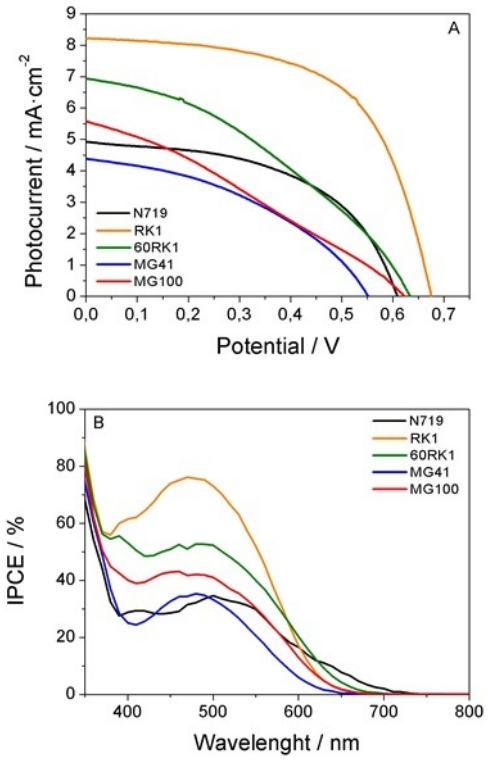

Fig. 4: (A) Current-voltage curves of the best performing device under 1 sun AM 1.5 illumination and (B) corresponding Incident Photon-to-Electron Conversion Efficiency spectra as a function of monochromatic wavelength for the dyes studied.

frontier orbitals of the dyes was determined by density functional theory (DFT) using the B3LYP hybrid functional. The calculated HOMO-LUMO gaps are shown in **Table 1**, where we observe the same trend as experimentally determined, i.e. **RK1** >**MG41**>**MG100**>**6ORK1**. The HOMO and LUMO energies and spatial representations of the two new dyes are shown on **Figure 3** and compared to those of **6ORK1.** The energy levels of LUMO and HOMO are well positioned with respect to the conduction band edge of the semiconductor (-0.4V versus NHE) and redox potential of I^-/I_3^- in the electrolyte (0.35V versus NHE). As a consequence, efficient electron injection and dye regeneration are expected. Moreover the LUMO constitution deserves some attention. For **MG41**, we see clearly LUMO extension on both cyanoacrylic groups. For **MG100**, we see absolutely no contribution from the PO_3H_2 group whereas for **6ORK1**, the LUMO has some extension over the COOH group. The contribution of the COOH to the LUMO is comprised between 2.21 and 4.51 % (See Supporting Information, Table S1). This contribution can be explained by the conjugation of the C=C bond with CN and of the C=O from CO_2H, whereas with the phosphonic group, no conjugation is expected.

Photovoltaic performance.

As reported in the literature, due to the low chemical stability of ZnO, the concentration of the dyes in solutions and the sensitization time are key factors for an optimal dye adsorption in the case of ZnO photoanodes.[20,21] In particular, due to the dissolution of ZnO by the acidic carboxylic groups of dyes, Zn^{2+}-dye complexes are produced, which can affect the electron injection kinetics.[22–24] For this reason, the sensitization time for a given dye concentration has been optimized prior to the characterization study (see Supporting Information, Figure S1). No significant differences were found in the first 3 hours for **RK1**-DSSCs. Nevertheless, for the rest of organic dyes a clear deterioration of the fill factor and even the short-circuit photocurrent was observed. The deterioration of these parameters could be attributed to a degradation of the electrodes during the staining step, because it is well-known that ZnO electrodes can be etched under acidic conditions.[22] To verify this hypothesis the pH of ethanol solution containing 0.2mM of each dye was measured. We found that the more acidic dyes are **MG41** and **MG100**, the less acidic one being **RK1**. Therefore a quicker degradation of the ZnO electrodes as a consequence of the dissolution of ZnO and formation of Zn^{2+}-dye aggregates during the dye sensitization[23,24] is expected with **MG100**, **MG41** and **6ORK1** that are more corrosive compared to **RK1**. Thus, for the preparation of the sensitized photoanodes later used in DSSCs, the sensitization time was restricted to only one hour, where a shorter period usually to sufficient adsorption of dyes on the mesoporous ZnO electrodes.[24]

In order to analyze the photovoltaic properties of the different dyes, the overall light conversion efficiency of ZnO-DSSC has been determined by means of I-V curve measurements. **Figure 4A** shows current-voltage characteristics of DSSCs employing a thin film (≈4 µm) of ZnO as photoanode sensitized with the different dyes. Bearing in mind the insensitivity of ZnO under the presence of *potential determining additives* reported recently,[19] the employed electrolyte in this work consists of only a redox pair (0.05M I_2 + 0.5M BMII) in acetonitrile as solvent electrolyte. The ruthenium dye **N719** has been used as sensitizer for the reference cell.

RSC Advances Accepted Manuscript

As shown in **Table 2**, the highest efficiency (3.3%) was found for **RK1**-DSSC. This efficiency is achieved by the combination of the highest photocurrent (8.2mA/cm^2) and photovoltage (675 mV). In addition, a rather good fill factor is obtained for **RK1**-DSSC, especially when it is compared to the other organic dyes. As a consequence of the low fill factor of **6ORK1**-DSSC, this dye shows a similar efficiency to **N719**-DSSC (1.7% and 1.6%, respectively) in spite of showing a higher photocurrent and photovoltage. On the other hand, **MG41**-DSSC and **MG100**-DSSC show a comparable photocurrent to **N719**-DSSC. Nevertheless, due to their low fill factor, these DSSCs show the lowest efficiencies (1%). Previous studies[29–31] have shown that higher rates of electron recombination lead to poor fill factors, which suggests that **6ORK1**-, **MG41**- and **MG100**-DSSC suffer a faster recombination. In addition, the fill factor may be lowered by the presence of dye aggregates in the pores impeding the transport of the redox couple, which is less of a factor for the RK-1 dye.

The short circuit photocurrent can be determined via

$$J_{SC} = q\int_{\lambda_{min}}^{\lambda_{max}} I_0(\lambda)\cdot IPCE(\lambda)\cdot d\lambda \qquad (Eq.1)$$

where *IPCE* is the incident photon-to-electron conversion efficiency, which is defined as the number of electrons generated in the solar devices with respect to the number of incident photons for a given wavelength, hence,

$$IPCE(\lambda) = \frac{n^o electrons}{n^o\ photons} = \frac{1240\cdot J_{sc}(\lambda)}{\lambda\cdot P_{light}(\lambda)} \qquad (Eq.2)$$

Dye	J_{sc} (mA/cm^{-2})	V_{oc} (mV)	Fill Factor (%)	Efficiency (%)
N719	4.9	610	52	1.6
RK1	8.2	675	60	3.3
6ORK1	6.9	630	39	1.7
MG41	4.4	555	41	1
MG100	5.6	620	30	1

Table 2: Photovoltaics parameters of the best performing device for each dye for a non-optimized architecture obtained under simulated AM 1.5 illumination

where $J_{sc}(\lambda)$ is the short-circuit photocurrent at a given wavelength (mA·cm^{-2}), λ is the wavelength (nm) of the incident light, P_{light} is the power of incident light (W·m^{-2}) and 1240 is a conversion factor. In particular, as shown in **Figure 4** the difference of short-circuit photocurrents is fully consistent with the differences of the IPCEs. **RK1**-DSSC, along with showing the higher photocurrent, shows an IPCE closer to 80% at the absorption maximum, whereas in the case of **N719**-DSSC an IPCE lower than 40% has been recorded. The IPCE depends on the efficiency of three different processes that determine the electrical conversion in a DSSC,

$$IPCE(\lambda) = \eta_{lh}(\lambda)\cdot\eta_g(\lambda)\cdot\eta_{col}(\lambda) \qquad (Eq.3)$$

where η_{lh} is the light harvesting efficiency, η_g is the generation efficiency of electrons under sunlight irradiation (including dye regeneration), and η_{col} is the charge collection efficiency from the device to the external circuit. Bearing in mind **Figure 2B**, **MG100**-DSSC shows the highest light harvesting efficiency. Nevertheless, **RK1**-DSSC, whose light harvesting efficiency is approximately similar to **MG100**-DSSC, shows the maximum IPCE. If good electron collection efficiency is assumed at short-circuit conditions,[8,32,33] two possible explanations could be suggested. First, **MG100** has the highest light harvesting efficiency but leads to a poor electron injection in the ZnO semiconductor or second, the dissolution of Zn^{2+} during the dye sensitization is more intense in the case of **MG100**. Taking into account the second assumption, a higher concentration of Zn^{2+}-dye complexes is accumulated in the pores of semiconductor. If it is assumed that the electron injection is only carried out by dye molecules directly attached to the ZnO surface, these complexes can only contribute to the light harvesting efficiency but not to the electron injection.[34] Both assumptions are probably related to the chemical nature of the phosphonic acid group that links this dye to the oxide, which may hinder the electronic overlap between the excited state of the dye and acceptor states in the oxide.

Optimization of architecture of dye-sensitized solar cell.

To optimize the energy conversion efficiency achieved in the previous section using **RK1** dye as sensitizer, different thicknesses of ZnO films have been tested. It should be kept in mind that the thickness of the mesoporous semiconductor films plays an important role in the performance of these solar devices because it determines the different photovoltaic parameters.[35,36] The thickness of the photoanode is very important to the adsorption of the dye and the electron recombination with the reduced species present in the electrolyte, which determine the J_{sc} and V_{oc} respectively. These two factors are intimately related to the surface area of semiconductor. It is expected that increased thickness will increase the photocurrent, due to the larger surface area available for the attachment of dye molecules. However, a decrease of the photovoltage is also expected as a consequence of the increase of electron recombination due to the increase of the semiconductor/electrolyte interfacial area. Figure S2 (see Supporting Information) confirms this expectation. Thus, bearing in mind the high absorption coefficient of **RK1** dye (**Figure 2A**), the thin film of 4 µm shows only a difference of 1.5 mA/cm^{-2} with respect to the thicker film of 8 µm. Therefore, an increase of the thickness contributes only to small increase of the photocurrent and an important efficiency loss due to the electron recombination. In contrast to the previous section, to guarantee the penetration of dye solution through the structure of photoanodes and to make sure that the entire surface in the thicker films is covered, a sensitization time of 90 min was used. **Figure 5** shows current-voltage characteristics of the optimal architecture for DSSCs employing an 8 µm thick ZnO film as

RSC Advances Accepted Manuscript

photoanode sensitized with the organic dye **RK1** and the ruthenium dye **N719**. In particular, RK1-DSSCs show a two-fold higher efficiency than for **N719**-DSSCs (3.7% and 1.7%, respectively). It should be noted that when TiO_2 is employed as photoanode, very similar solar cell performances have been achieved for both dyes (See Supporting Information, Figure S3). In **Figure 5**, **RK1**-DSSCs show a short-circuit photocurrent of 9.3 mA/cm^{-2} whereas in the case of **N719**-DSSCs values of 5.2 mA/cm^{-2} has been found. The effect of surface area is intimately related with the average particle size, which is relatively large for the ZnO particles used in this work (40 - 100 nm), resulting in a BET surface area of 4m^{2}g^{-1}. This surface area is significantly lower than for TiO_2 DSSCs, where the BET surface area is generally about 80m^{2}g^{-1}. Hence, the much higher absorption coefficient of the organic dyes used here is essential for the performance of the solar cells, also because the film thickness is similar as generally applied in TiO_2 DSSCs. On the other hand, it was observed from desorption measurements that the RK1 dye adsorbs at ZnO at a higher coverage than the N719 dye by a factor of 1.7 (See Supporting Information, Figure S4), which also directly benefits the efficiency of the RK1-sensitized ZnO DSSCs. These observations also explain why the difference in efficiency for TiO_2 DSSCs with the RK1 and N719 dyes is much less pronounced, as the surface area is much larger and does not limit cell performance.

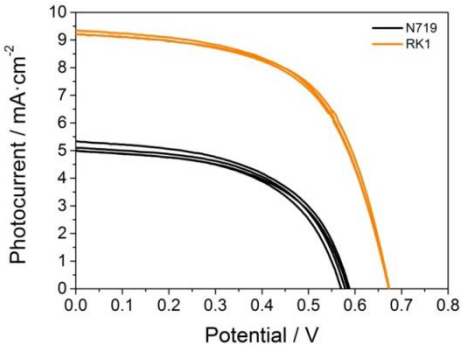

Fig. 5: Current-voltage curves under 1 sun AM 1.5 illumination for RK1 and N719 using a 8µm ZnO film as photoanode.

This difference is consistent with the IPCE showed in **Figure 4B** where values approximately two times higher were reported. However, the open-circuit photovoltage is also greatly increased when **RK1** (675mV) is used as sensitizer with respect to **N719** dye (585mV). To cast light on this remarkable effect, an electrochemical impedance spectroscopy (EIS) study has been performed.[37,38] By means of EIS the two factors that determine the electron lifetime (τ_n) via **Equation 4**, and then the open-circuit photovoltage, are analyzed: (1) the position of the conduction band edge by means of the chemical capacitance, C_μ, and (2) the electron recombination resistance, R_{rec}.

$$\tau_n^{EIS} = C_\mu \cdot R_{rec} \qquad (Eq.4)$$

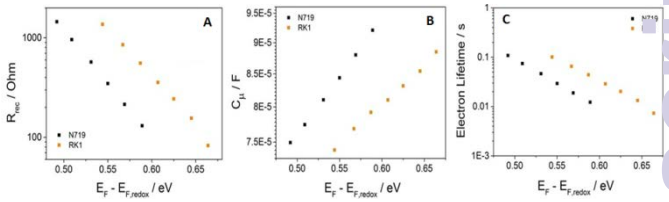

Fig.6: (A) Electron recombination resistance, (B) chemical capacitance and (C) electron lifetime data as extracted from EIS measurements in **RK1**-DSSC and **N719**-DSSC based on ZnO.

In **Figure 6**, the electron recombination resistance, chemical capacitance and the electron lifetime extracted from the EIS spectra at different potential ($E_F - E_{F\text{-}redox}$) are reported.

Figure 6A shows a higher electron recombination resistance for **RK1**-DSSC than for **N719**-DSSC at a given value of the Fermi level. On the other hand, the chemical capacitance data (**Figure 6B**) evidences a clear difference between RK1-DSSC and N719-DSSC. Similar results were found for TiO_2-DSSC (see Supporting Information, Figure S5). It means that the adsorption of these dyes on the semiconductor surface produces a shift of position of the conduction band edge with respect to E_{redox} of the electrolyte. In particular, a negative band-shift in the semiconductor oxide band edge has been found for **RK1**-DSSC with respect to **N719**-DSSC. Therefore, the energy difference between the conduction band edge and E_{redox} of electrolyte, which is the other factor that determines the open-circuit photovoltage, is higher for **RK1**-DSSCs. The electron lifetime extracted via Equation 4, as shown in **Figure 6C**, is larger for **RK1**-DSSC compared to **N719**-DSSC. Consequently, **RK1**-DSSC shows a higher open-circuit photovoltage. These results are supported by the electron lifetimes extracted from OCVD measurements (Supporting Information, Figure S6).[39,40]

Nevertheless, to determine the origin of the longer electron lifetime, it is necessary to distinguish between the thermodynamic effect (chemical capacitance) and kinetic effect (electron recombination resistance). Hence, it is necessary to separate out the thermodynamic effects from the electron recombination rate and compare the electron recombination resistances at the same value of the total electron density stored in the semiconductor oxide. In this work this correction has been applied by looking at the shift of the capacitance lines detected in the EIS measurements. Shifting the potential to a value at which all capacitance lines overlap, one makes sure that the electron recombination resistance is plotted at the same value of the total electron density ($E_{F(shift)} - E_{F\text{-}redox}$). Once the band-shift according to chemical capacitance data is corrected, a slightly lower electron recombination resistance was estimated for **RK1**-DSSC in comparison to **N719**-DSSC (Supporting Information, Figure S7). Therefore, bearing in mind that the kinetics of electron recombination at the same value of electron densit

RSC Advances Accepted Manuscript

This journal is © The Royal Society of Chemistry 20xx

are very similar for both dyes, the band-shift of the semiconductor oxide is the main factor responsible for the different open-circuit photovoltage in both DSSCs.

Conclusions

Since the optimization of electrolyte composition by the addition of potential-determining additives does not represent a way to improve the efficiency of ZnO-DSSC, the search for new dyes with a higher absorption coefficient can be considered as an alternative strategy. In this work, the photovoltaic performances of different donor-π-acceptor organic dyes have been studied and compared with the most common ruthenium dye **N719**. The organic dyes are derivatives of **RK1**, which is a promising organic dye for DSSC applications. The main structural differences of the dye molecules obtained reside in the substitution of the triphenylamine unit and the number and nature of anchoring groups. The difference in their photovoltaic performances has been attributed to their different light harvesting efficiencies. In relation to the interaction between the dyes and ZnO surface, the use of $–PO_3H_2$ moiety as anchoring group appears to be connected with a more intense edging of the ZnO semiconductor surface and/or a poorer electron injection rate as compared to the –COOH groups.

After the optimization of the architecture of DSSCs, using the **RK1** organic dye as sensitizer an overall light conversion efficiency of 3.7% has been achieved. In spite of showing similar electron recombination kinetics to **N719** dye, due to the higher absorption coefficient of **RK1** dye and the induced negative band-shift of the conduction band edge of the ZnO semiconductor, a higher photocurrent and photovoltage is demonstrated. In particular, the efficiency becomes more than twice as high as for the **N719** dye studied under the same conditions when ZnO as photoanode is used as photoanode.

Experimental section

Synthesis of the dyes.

General. Tri(o-tolyl)phosphine, tris(dibenzylideneacetone)di-palladium(0), 3,5-diformyl-phenyl-boronic acid, palladium acetate (II), diethyl cyanomethylphosphonate, trimethylsilyl iodide, 2-cyanoacetic acid and piperidine were purchased from Aldrich or TCI chemicals and used as received. Tripotassium phosphate was obtaninedfrom Acros Organics and 4,7-dibromo-2,1,3-benzothiadiazole from Orgalight. The solvents, such as anhydrous toluene, chloroform, dichloromethane, isopropanol and acetonitrile were purchased from Aldrich and used as received. Spectroscopic grade solvents from Aldrich were used for spectral measurements. Compounds **1** and **4** were synthesised according to literature.[27]

Synthesis of 2: Under argon, compound **1** (200 mg, 0.31 mmol, 1.0 equiv.) was dissolved in distilled THF (5.0 mL) then a 1.5 M solution of n-BuLi (250 µL, 0.37 mmol, 1.2 equiv.) was added at -78 °C. The solution was stirred for an hour at -50 °C before adding a 1.0 M n-hexane solution of Me_3SnCl (406 µL, 0.41 mmol, 1.3 equiv) at -78 °C. The solution was allowed to reach room temperature and was stirred for 2 hours. The reaction was quenched with NH_4Cl and the organic phase was extracted with n-hexane, dried with Na_2SO_4, filtered and concentrated under vacuum. The resulting mixture was engaged without any further purification in a Stille coupling with 4,7-dibromo-2,1,3-benzothiadiazole. Under argon, the stannic compound and 4,7-dibromo-2,1,3-benzothiadiazole (86 mg, 0.31 mmol, 1.0 equiv), Pd_2dba_3 (7 mg, 0.01 mmol, 4 % mol) and P(o-tolyl)$_3$ (29 mg, 0.09 mmol, 0.3 equiv) were dissolved in anhydrous toluene (5.0 mL) and refluxed for 19 hours. The mixture was then poured into HCl (2 M). The organic phase was extracted with Et_2O, washed with HCl (2 M), dried over Na_2SO_4 and concentrated. The residue was purified by silica gel column chromatography (Pentane/CH_2Cl_2, 7:3) to obtain the desired product **2** (130 mg, yield = 49 %) as a red film.

^{1}H NMR ($CDCl_3$, 200 MHz) δ (ppm): 7.99 (s, 1 H), 7.83 (d, *J* = 7.8 Hz, 1 H), 7.67 (d, *J* = 7.8 Hz, 1 H), 7.28 (d, *J* = 8,5 Hz, 2 H), 7.10 (d, *J* = 8.5 Hz, 4 H), 6.94 (d, *J* = 8.4 Hz, 2 H), 6.85 (d, *J* = 8.8 Hz, 4 H), 3.94 (t, *J* = 6.5 Hz, 4 H), 2.72 (m, 2 H), 1.87-1.60 (m, 6 H), 1.52-1.22 (m, 22 H), 0.98-0.81 (m, 9 H). ^{13}C NMR ($CDCl_3$, 100 MHz) δ (ppm): 155.9, 154.0, 152.0, 148.6, 140.8, 140.5, 139.3, 135.4, 132.5, 131.2, 129.8, 127.5, 127.1, 125.2, 119.7, 115.5, 111.7, 68.4, 32.0, 31.8, 31.2, 29.7, 29.6, 29.5, 29.1, 25.9, 22.8, 22.8, 14.3, 14.2. Anal.Calcd for $C_{48}H_{58}N_3O_2BrS_2$: C, 67.59; H, 6.85; N, 4.93; S, 7.52. Found: C, 67.47; H, 6.99; N, 4.66; S, 7.24.

Synthesis of 3: A mixture of **2** (100 mg, 0.12 mmol, 1 equiv.), 3,5-diformylphenylboronic acid (31 mg, 0.18 mmol, 1.5 equiv.), $Pd(OAc)_2$ (1.0 mg, 2.0 µmol, 2 mol%), K_3PO_4 (50 mg, 0.23 mmol, 2 equiv.), THF (2 mL), iPrOH (1 mL) and distilled water (1 mL) was stirred at 80 °C for 62 hours under air. The mixture was added to brine and extracted four times with ethyl acetate. Combined organic phases were dried over Na_2SO_4, filtered and concentrated under reduced pressure. The resulting mixture was purified by silica gel column chromatography (Hexane/EtOAc, 8:2) to obtain the desired product as a red solid **3** (63 mg, yield = 66%).

^{1}H NMR ($CDCl_3$, 200 MHz) δ (ppm): 10.2 (s, 2 H), 8.80 (s, 2 H), 8.43 (s, 1 H), 8.09 (s, 1 H), 7.94 (d, *J* = 7.5 Hz, 1 H), 7.85 (d, *J* = 7.5 Hz, 1 H), 7.32 (d, *J* = 8.7 Hz, 2 H), 7.11 (d, *J* = 8.9 Hz, 4 H), 6.96 (d, *J* = 8.7 Hz, 2 H), 6.85 (d, *J* = 8.9 Hz, 4 H), 3.93 (t, *J* = 6.5 Hz, 4 H), 2.75 (m, 2 H), 1.88-1.62 (m, 6 H), 1.56-1.20 (m, 22 H), 0.98-0.82 (m, 9 H). ^{13}C NMR ($CDCl_3$, 100 MHz) δ (ppm): 191.0, 155.8, 153.5, 152.6, 148.5, 141.0, 140.3, 139.4, 139.2, 137.4, 135.5, 135.0, 131.3, 129.9, 129.6, 128.8, 128.6, 128.2, 127.0, 125.6, 124.5, 119.5, 115.4, 68.3, 31.9, 31.6, 31.1, 29.6, 29.4, 29.3, 29.3, 29.0, 25.8, 22.7, 22.6, 14.1, 14.1. Anal.Calcd for $C_{56}H_{63}N_3O_4S_2$: C, 74.22; H, 7.01; N, 4.64; S, 7.08. Found: C, 74.59; H, 7.16; N, 4.58; S, 7.05.

Synthesis of MG41: The compound **3** (50 mg, 0.06 mmol, 1 equiv) and cyanoacetic acid (47 mg, 0.55 mmol, 10 equiv.) were dissolved in a mixture of acetonitrile (6 mL) and chloroform (3 mL). A few drops of piperidine were added and the reaction mixture was stirred at reflux for 15 hours

RSC Advances Accepted Manuscript

Solvents were removed under reduced pressure. The solid was taken in chloroform, washed with HCl (2M), dried over Na_2SO_4, filtered and concentrated under reduced pressure. The residue was purified by silica gel column chromatography (CH_2Cl_2/MeOH/AcOH, 1:0:0 to 90:5:5) to obtain the desired red solid **MG41** (50 mg, yield = 81 %).

^{1}H NMR (THF-d_8, 200 MHz) δ (ppm): 9.05 (s, 2 H), 8.49 (s, 1 H), 8.43 (s, 2 H), 8.20 (s, 1 H), 8.10 (d, *J* = 7.6 Hz, 1 H), 8.00 (d, *J* = 7.6 Hz, 1 H), 7.32 (d, *J* = 8.6 Hz, 2 H), 7.07 (d, *J* = 9.0 Hz, 4 H), 6.92 (d, *J* = 9.0 Hz, 2 H), 6.85 (d, *J* = 9.0 Hz, 4 H), 3.94 (t, *J* = 6.2 Hz, 4 H), 2.76 (m, 2 H), 1.85-1.67 (m, 6 H), 1.59-1.21 (m, 22 H), 1.00-0.81 (m, 9 H). ^{13}C NMR (THF-d_8, 50 MHz) δ (ppm): 238.6, 163.3, 157.0, 154.5, 153.5, 153.4, 149.6, 141.7, 141.2, 140.0, 139.6, 136.8, 134.6, 134.2, 133.3, 132.0, 130.3, 130.0, 129.7, 129.4, 128.7, 127.8, 126.8, 126.6, 125.5, 125.5, 120.1, 116.0, 115.8, 107.2, 107.2, 68.7, 32.9, 32.6, 31.9, 30.6, 30.5, 30.4, 30.3, 30.3, 29.8, 26.7, 23.5, 14.5, 14.4. HRMS (ESI): $[M\text{-}H]^+$= 1039.4368 (calcd. for $C_{62}H_{65}N_5O_6S_2$: 1039.4371).

Synthesis of 5: The compound **4** (120 mg, 0.14 mmol, 1.0 equiv.) and diethyl cyanomethylphosphonate (111 µL, 0.68 mmol, 5.0 equiv.) were dissolved in a mixture of acetonitrile (10 mL) and chloroform (5 mL). A few drops of piperidine were added and the reaction mixture was stirred at reflux for 3 hours. The resulting mixture was washed with water then brine. The organic phase was dried over Na_2SO_4, filtered and concentrated under reduced pressure. The residue was purified by silica gel column chromatography (Hexane/EtOAc, 7:3 to 1:1) to obtain the desired red film **5** (80 mg, yield = 52 %).

^{1}H NMR ($CDCl_3$, 400 MHz) δ (ppm): 8.18-8.08 (m, 4 H), 8.07 (d, *J* = 8.4 Hz, 2 H), 7.93 (d, *J* = 7.5 Hz, 1 H), 7.80 (d, *J* = 7.6 Hz, 1 H), 7.32 (d, *J* = 8.7 Hz, 2 H), 7.11 (d, *J* = 8.9 Hz, 4 H), 6.96 (d, *J* = 8.7 Hz, 2 H), 6.85 (d, *J* = 9.0 Hz, 4 H), 4.34-4.19 (m, 4 H), 3.95 (t, *J* = 6.5 Hz, 4 H), 2.75 (t, *J* = 7.9 Hz, 2 H), 1.83-1.67 (m, 6 H), 1.52-1.23 (m, 28 H), 0.95-0.85 (m, 9 H). ^{13}C NMR ($CDCl_3$, 50 MHz) δ (ppm): 158.4, 155.8, 153.8, 148.5, 142.1, 141.0, 140.4, 139.3, 135.9, 131.9, 131.3, 131.0, 130.2, 129.9, 129.8, 129.0, 128.0, 127.1, 125.7, 124.9, 119.7, 115.4, 97.9, 68.4, 63.9, 63.8, 32.0, 31.7, 31.2, 29.7, 29.5, 29.1, 25.9, 22.8, 16.5, 16.4, 14.2. Anal.Calcd for $C_{61}H_{73}N_4O_5PS_2$: C, 70.63; H, 7.09; N, 5.40; S, 6.18. Found: C, 70.82; H, 7.21; N, 5.17; S, 5.87.

Synthesis of MG100: To a solution of compound **5** (130 mg, 0.13 mmol, 1.0 equiv.) in 15 mL of CH_2Cl_2, TMSI (107 µL, 0.75 mmol, 6.0 equiv.) was added dropwise under argon at room temperature. The mixture was then stirred at room temperature for 15 h. The solvents were removed under reduced pressure to dryness. The residue was then diluted in 100 mL of MeOH and dried under vacuum. The desired product **MG100** was then obtained as a red solid (115 mg, yield = 93 %) after washing with pentane.

^{1}H NMR (THF-d_8, 400 MHz) δ (ppm): 8.15 (d, *J* = 8.54 Hz, 2 H), 8.11 (s, 1 H), 8.05 (d, *J* = 8.5 Hz, 2 H), 7.97 (d, *J* = 19.8 Hz, 1 H), 7.85 (d, *J* = 7.5 Hz, 1 H), 7.77 (d, *J* = 7.6 Hz, 1 H), 7.28 (d, *J* = 8.8 Hz, 2 H), 7.06 (d, *J* = 9.0 Hz, 4 H), 6.91 (d, *J* = 8.8 Hz, 2 H), 6.85 (d, *J* = 9.0 Hz, 4 H), 3.94 (t, *J* = 6.4 Hz, 4 H), 2.71 (m, 2 H), 1.83-1.66 (m, 6 H), 1.55-1.44 (m, 4 H), 1.44-1.22 (m, 18 H), 0.98-0.83 (m, 9 H). ^{13}C NMR (THF-d_8, 100 MHz) δ (ppm): 156.8, 154.3, 153.2, 149.3, 141.6, 141.3, 141.1, 139.4, 136.6, 131.8, 131.8, 130.8, 130.6, 130.1, 130.1, 129.3, 129.3, 128.1, 127.6, 126.5, 125.0, 120.1, 115.9, 68.6, 32.7, 32.4, 31.8, 30.4, 30.3, 30.1, 29.7, 26.6, 23.4, 14.3, 14.2. HRMS (ESI): $[M\text{-}H]^-$= 979.4068 (calcd. for $C_{57}H_{64}N_4O_5PS_2$: 979.4061).

Fabrication of Dye-Sensitized Solar Cells.

The working electrodes were made from ZnO nanoparticles (40 - 100 nm) prepared by a forced hydrolysis method (see Supporting Information, Figure S8).[41] The BET surface area was 4 ± 2m^2g^{-1}, which is significantly lower than generally used for TiO_2 DSSCs, where the BET area is generally around 80m^2g^{-1}. Different thicknesses of ZnO photoanodes were deposited. Prior to the deposition of the paste the conducting glass substrates (*Pilkington - TEC15*) were heated to 500°C. The nanoparticle pastes were deposited onto a conducting glass substrate using the screen printing technique. The DSSC active area was 0.16 cm^2. The films were gradually heated under airflow up to 450°C for ZnO electrodes. The counter-electrodes were made by spreading a Platisol solution (*Solaronix*) onto a conducting glass substrate (*Pilkington - TEC8*) followed by heating at 390°C for 15 minutes.[42]

The working electrodes were immersed in a solution containing different organic dyes employed in this study. These solutions contained 0.5 mM dye and 5 mM chenodeoxycholic acid in ethanol.[17] In contrast, a solution containing 0.5 mM dye and 0.5 mM chenodeoxycholic acid in ethanol was used for the ruthenium dye. After the sensitization, the electrodes were washed with ethanol and dried in air. Finally, the working and counter electrodes were sandwiched together using a hot melt film (*Surlyn*, *Solaronix*). The cells were filled with the electrolyte through a hole previously made in the back of a platinized counter electrode using vacuum. Then, the hole was sealed with a hot melt film and a cover glass.

Characterization of solar cells.

The devices were characterized using a solar simulator with AM 1.5G filter (*ABET*). The light intensity was calibrated to the standard value of 1 Sun (100 mW/cm^2) using a reference solar cell with temperature output (*Oriel, 91150*). The current-voltage characteristics were determined by applying an external potential bias to the cell and measuring the photocurrent using an *Autolab/PGSTAT302N*potentiostat. Open-circuit Voltage Decay (OCVD) measurements were performed by keeping the solar cell at open-circuit at 1 sun and recording the voltage decay after interrupting the illumination.

OCVD and Electrochemical Impedance Spectroscopy (EIS) were utilized to extract electron lifetimes, electron recombination and chemical capacitance. The illumination for the small perturbation (frequency response) technique (EIS) was provided by a 530 nm light emitting diode (*LUXEON*) over a

RSC Advances Accepted Manuscript

This journal is © The Royal Society of Chemistry 20xx

wide range of DC light intensities. The technique allows probing the device performance at different positions of the Fermi level in the semiconductor. A response analyzer module (*PGSTAT302N/FRA2, AutoLab*) was utilized to analyze the frequency response of the devices. To avoid voltage drop due to series resistance EIS measurements were performed at the open circuit conditions and the Fermi level (related to the open-circuit voltage) was fixed by the DC illumination intensity. A 10 mV perturbation in the 10^{-5} to 10^{-2} Hz range was utilized to obtain the EIS spectra. Zview equivalent circuit modelling software (*Scribner*) was used to fit the EIS spectra, including the distributed element DX11 (transmission line model). In all cases the samples were illuminated from the dye-coated electrode side.

Incident photon-to-electron conversion efficiencies (IPCE) were measured by means of an Oriel Xenon lamp coupled to a 0.2 m monochromator (*McPherson*). The light intensity was determined as a function of the wavelength using a calibrated silicon photodiode (*PH-100 Si, GENTECE*).

UV-Vis absorption spectra of dye solutions were recorded on a Perkin-Elmer Lambda 2 spectrometer (wavelength range: 180-820 nm; resolution: 2 nm), the spectra of ZnO sensitized films were recorded using an 50mm integrating sphere (*Ocean Optics*). For dye loading measurements, a solution of 0.1M KOH in methanol was used. Electrochemical studies of the organic dyes were carried out in a one compartment, three-electrode electrochemical cell equipped with a flat platinum working electrode (7 mm^2), a Pt wire counter electrode, and a Ag wire pseudo-reference electrode, whose potential was checked using the Fc/Fc^+ couple as an internal standard. The electrolyte was prepared using 0.2 M tetrabutylammoniumhexafluorophosphate (Bu_4NPF_6) solution in dichloromethane containing 2 x 10^{-3} M of the dye.

Computational details

The procedure for geometry optimizations and examination of the resulting electronic structures has been described elsewhere.[27] We have replaced the hexyl chains by methyl functions to save computational efforts. For all the molecules described here, we have explored both cis and trans conformations, with respect to the dihedral angle between the thiophene and benzothiadiazole group. The main characteristics of cis/trans conformers are essentially the same: similar stabilization energies in a 0.05 eV range, HOMO/LUMO energies within 0.02 eV and % contributions of LUMOs within 1%.

Acknowledgements

Conacyt is gratefully acknowledged for funding under grant CB-2012-178510 and Conacyt/SENER and IER-UNAM for funding through the Mexican Center for Innovation in Solar Energy (CeMIE-Sol), Project P-27. We would also like to acknowledge the invaluable help of Beatriz Heredia Cervera. We thank Junta de Andalucía for financial support via grant FQM 1851. We thank Ministerio de Economía y Competitividad of Spain under grant MAT2013-47192-C3-3-R**.** MG and RD thank CNRS and CEA for partial funding. RD and DJ acknowledge the European Union Research Executive Agency for funding through the Adios-Ru research project. This project is funded by the European Union Research Executive Agency (contract 315131) on the Research for SMEs programme.

Notes and references

1 B. O'Regan and M. Gratzel, *Nature*, 1991, **353**, 737–740.
2 M. Grätzel, *Acc. Chem. Res.*, 2009, **42**, 1788–1798.
3 Y. Liu, J. R. Jennings, Y. Huang,Q. Wang, S. M. Zakeeruddin and M. Grätzel, *J Phys Chem C*, 2011, **115**, 18847–18855.
4 B. E. Hardin, H. J. Snaith and M. D. McGehee, *Nat. Photonics*, 2012, **6**, 162–169.
5 H. J. Snaith, *J. Phys. Chem. Lett.*, 2013, **4**, 3623–3630.
6 J.-H. Im, C.-R. Lee, J.-W. Lee, S.-W. Park and N.-G. Pa *Nanoscale*, 2011, **3**, 4088–4093.
7 F. Gao, Y. Wang, D. Shi, J. Zhang, M. K. Wang, X. Y. Jing, R. Humphry-Baker, P. Wang, S. M. Zakeeruddin and M. Gratzel, *J. Am. Chem. Soc.*, 2008, **130**, 10720–10728.
8 A. Hagfeldt, G. Boschloo, L. Sun, L. Kloo and H. Pettersson, *Chem. Rev.*, 2010, **110**, 6595–6663.
9 W. D. Zeng, Y. M. Cao, Y. Bai, Y. H. Wang, Y. S. Shi, M. Zhang, F. F. Wang, C. Y. Pan and P. Wang, *Chem. Mater.*, 2010, **22**, 1915–1925.
10 A. Yella, H.-W. Lee, H. N. Tsao, C. Yi, A. K. Chandiran, M. K. Nazeeruddin, E. W.-G. Diau, C.-Y. Yeh, S. M. Zakeeruddin and M. Grätzel, *Science*, 2011, **334**, 629–634.
11 A. Mishra, M. K. R. Fischer and P. Bäuerle, *Angew. Chem. Int. Ed.*, 2009, **48**, 2474–2499.
12 M. Liang and J. Chen, *Chem. Soc. Rev.*, 2013, **42**, 3453–3488.
13 S. Ito, H. Miura, S. Uchida, M. Takata, K. Sumioka, P. Liska, P. Comte, P. Pechy and M. Graetzel, *Chem. Commun.*, 2008, 5194–5196.
14 A. Dualeh, F. De Angelis, S. Fantacci, T. Moehl, C. Yi, F. Kessler, E. Baranoff, M. K. Nazeeruddin and M. Grätzel, *J. Phys. Chem. C*, 2012, **116**, 1572–1578.
15 G. Cicero, G. Musso, A. Lamberti, B. Camino, S. Bianco, D. Pugliese, F. Risplendi, A. Sacco, N. Shahzad, A. M. Ferrari, B. Ballarin, C. Barolo, E. Tresso and G. Caputo, *Phys Chem Chem Phys*, 2013, **15**, 7198–7203.
16 Y. Ooyama and Y. Harima, *ChemPhysChem*, 2012, **13**, 4005–4005.
17 D. Joly, L. Pellejà, S. Narbey, F. Oswald, J. Chiron, J. N. Clifford, E. Palomares and R. Demadrille, *Sci Rep*, 2014, **4**.
18 J. Sobuś, G. Burdziński, J. Karolczak, J. Idígoras, J. A. Anta and M. Ziółek, *Langmuir*, 2014, **30**, 2505–2512.
19 J. Idígoras, G. Burdziński, J. Karolczak, J. Kubicki, G. Oskam, J. A. Anta and M. Ziółek, *J. Phys. Chem. C*, 2015, **119**, 3931–3944.
20 E. Guillen, F. Casanueva, J. A. Anta, A. Vega-Poot, G. Oskam, R. Alcantara, C. Fernandez-Lorenzo and J. Martin-Calleja, *J. Photochem. Photobiol. -Chem.*, 2008, **200**, 364–370.
21 T. P. Chou, Q. Zhang and G. Cao, *J. Phys. Chem. C*, 2007, **111**, 18804–18811.
22 R. Katoh, A. Furube, Y. Tamaki, T. Yoshihara, M. Murai, K. Hara, S. Murata, H. Arakawa and M. Tachiya, *Sixth AIST Int. Symp. Photoreact. Control Photoreact. Mater.*, 2004, **166**, 63–74.

RSC Advances Accepted Manuscript

23 K. Keis, J. Lindgren, S. E. Lindquist and A. Hagfeldt, *Langmuir*, 2000, **16**, 4688–4694.
24 A. Lamberti, R. Gazia, A. Sacco, S. Bianco, M. Quaglio, A. Chiodoni, E. Tresso and C. F. Pirri, *Prog. Photovolt. Res. Appl.*, 2014, **22**, 189–197.
25 N. Memarian, I. Concina, A. Braga, S. M. Rozati, A. Vomiero and G. Sberveglieri, *Angew. Chem. Int. Ed Engl.*, 2011, **50**, 12321–12325.
26 D. Barpuzary, A. S. Patra, J. V. Vaghasiya, B. G. Solanki, S. S. Soni and M. Qureshi, *ACS Appl. Mater. Interfaces*, 2014, **6**, 12629–12639.
27 D. Joly, L. Pellejà, S. Narbey, F. Oswald, T. Meyer, Y. Kervella, P. Maldivi, J. N. Clifford, E. Palomares and R. Demadrille, *Energy Environ. Sci.*, 2015, **8**, 2010–2018.
28 S. Buathong, D. Ung, T. J. Daou, C. Ulhaq-Bouillet, G. Pourroy, D. Guillon, L. Ivanova, I. Bernhardt, S. Bégin-Colin and B. Donnio, *J. Phys. Chem. C*, 2009, **113**, 12201–12212.
29 B. C. O'Regan and F. Lenzmann, *J. Phys. Chem. B*, 2004, **108**, 4342–4350.
30 J. Bisquert and I. Mora-Seró, *J. Phys. Chem. Lett.*, 2010, **1**, 450–456.
31 J. A. Anta, J. Idígoras, E. Guillén, J. Villanueva-Cab, H. J. Mandujano-Ramírez, G. Oskam, L. Pellejà and E. Palomares, *Phys. Chem. Chem. Phys.*, 2012, **14**, 10285–10299.
32 L. M. Peter, *J. Phys. Chem. C*, 2007, **111**, 6601–6612.
33 J. A. Anta, E. Guillén and R. Tena-Zaera, *J. Phys. Chem. C*, 2012, **116**, 11413–11425.
34 H. Horiuchi, R. Katoh, K. Hara, M. Yanagida, S. Murata, H. Arakawa and M. Tachiya, *J. Phys. Chem. B*, 2003, **107**, 2570–2574.
35 Z. Longyue, D. Songyuan, X. Weiwei and W. Kongjia, *Plasma Sci. Technol.*, 2006, **8**, 172.
36 W. H. Chiu, C. H. Lee, H. M. Cheng, H. F. Lin, S. C. Liao, J. M. Wu and W. F. Hsieh, *Energy Environ. Sci.*, 2009, **2**, 694–698.
37 F. Fabregat-Santiago, J. Bisquert, G. Garcia-Belmonte, G. Boschloo and A. Hagfeldt, *Sol. Energy Mater. Sol. Cells*, 2005, **87**, 117–131.
38 J. Bisquert, *J. Phys. Chem. B*, 2002, **106**, 325–333.
39 A. Zaban, M. Greenshtein and J. Bisquert, *Chemphyschem*, 2003, **4**, 859–864.
40 M. Ansari-Rad, Y. Abdi and E. Arzi, *J Phys Chem C*, 2012, **116**, 10867–10872.
41 A. G. Vega-Poot, M. Macías-Montero, J. Idígoras, A. Borrás, A. Barranco, A. R. Gonzalez-Elipe, F. I. Lizama-Tzec, G. Oskam and J. A. Anta, *ChemPhysChem*, 2014, **15**, 1088–1097.
42 A. Reynal, A. Forneli and E. Palomares, *Energy Env. Sci*, 2010, **3**, 805–812.

RSC Advances Accepted Manuscript

This journal is © The Royal Society of Chemistry 20xx